Journal of Applied Sciences

ISSN 1812-5654

science alert

ANSInet
an open access publisher
http://ansinet.com

Journal of Applied Sciences 10 (20): 2379-2386, 2010
ISSN 1812-5654

Design and Optimization of a Radial Flux Direct-drive PM Generator using Ant Colony Algorithm

[1]A. Zabihinejad and [2]M.E. Iranian
[1]Mapna Electrical and Control, Engineering and Manufacturing Company,
42, Ziba St., Keshavarz Bulvar, Tehran, Iran
[2]Mapna Electrical and Control Engineering and Manufacturing Company,
27th Ashouri St., East Kaveh Ave Namjoo Sq, Tehran, Iran

Abstract: This study discussed the development of a high power Radial flux direct-drive PM generator for wind applications. A low-speed radial-flux permanent-electrical with new magnet (PM) generator topology was built and tested. The designed, optimized and constructed. This study presents the design of a 20 kW permanent magnet generator using Neodymium-Iron-Boron. The Finite Element Technique (FET) is used for detailed characteristics and final adjustments. The design was carried out with high-energy NdFeB built and tested. The ant colony algorithm is used to optimize machine structure and to achieve high power density and efficiency. The generator operation is investigated in both simulation and implementation. The simulation results show that the optimized structure have higher efficiency in comparison with other optimization methods such as genetic algorithm. The great agreement between simulation and implementation results proves the validity of this generator structure.

Key words: Ant colony optimization, direct-drive, finite element method, PM generator

INTRODUCTION

Recently, a great attention has been paid to the pollution-free renewable energy sources to be an alternative source for oil, gas, Uranium and coal sources that will last no longer than one century. Boldea and Nasar (1987) introduce the wind energy as one of the most important types of renewable energy sources that have been used widely in electricity generation. The fact is that the cost of energy supplied by wind turbines is continuously decreasing.

Wind generators using radial flux configuration become more and more popular. Joorabian and Zabihinejad (2009) and Kang *et al.* (2000) showed that drop in prices of rare-earth Permanent Magnet (PM) materials and progress in power electronics have played an important role in the development of PM synchronous machines in the last three decades. Mirzayee *et al.* (2005) and Kang *et al.* (2000) compared the traditional machines using gearbox to couple to wind turbines with direct-drive generators which present some advantages such as producing higher efficiency, operating with similar magnetic flux density in all the magnetic circuit and allowing the construction of compact generators with a large number of poles.

Boldea and Nasar (1987) and Muljadi *et al.* (1999) introduce the conventional generators which are installed at the top of the towers and require step-up gearbox so that the type of generator for this application needs to be compact and light. The gearbox of a wind generator is expensive, subject to vibration, noise and fatigue and needs lubrication as well as maintenance at appreciable cost.

Joorabian and Zabihinejad (2009), Chen *et al.* (2000), Gieras and Gieras (2002) and Gieras *et al.* (2004) showed that Radial flux permanent magnet generator has higher efficiency in comparison with conventional doubly fed induction generators. But design of these generators is so complex. Kessinger and Robinson (1997) and Kessinger *et al.* (1998) proved that it is more difficult to design a high mechanical integrity rotor-shaft mechanical joint in the higher range of the output power. A common solution to the improvement of the mechanical integrity of the rotor-shaft joint is to design multidisc (multi-stage) machine. In the Radial structures, output power can increase easily by increasing the stator length.

Dorigo *et al.* (1991, 1996) and Dorigo (1992) presented Ant Colony Optimization (ACO) such as a pattern solution for combinatorial optimization problems. The first algorithm which can be classified with in this framework

Corresponding Author: Amin Zabihinejad, Mapna Electrical and Control, Engineering and Manufacturing Company, 42, Ziba St., Keshavarz Bulvar, Tehran, Iran Tel: +98 937 803 0478

was presented by Dorigo *et al.* (1991) and Di Caro and Dorigo (1998) and since then, many diverse variants of the basic principle have been reported in the literature.

The characteristic of ACO algorithms is their explicit use of elements of previous solutions. In fact, they drive a constructive low-level solution. But including it in a population framework and randomizing the construction in a Monte Carlo way. Stutzle and Hoos (1998) and Tsekouras *et al.* (2001) suggested a Monte Carlo combination of different solution elements also by Genetic Algorithms but in the case of ACO the probability distribution is explicitly defined by previously obtained solution components.

So far no significant effort has been made to develop high power Radial Flux Permanent Magnet (RFPM) synchronous generators for directly coupling with wind turbines. In this study, complete design and optimization procedures for such electric machine are developed and the manufacturing aspects for the construction of a 20 kW, 150 rpm, 50 Hz prototype are discussed. Since, this generator is a direct-drive generator, a rectifier-converter set is required to connect it with the power system.

Ant Colony Optimization (ACO): ACO algorithms simulate the behavior of real ants. They are based on the principle that using simple communication mechanisms, an ant group is able to find the shortest path between any two points. During their trips, a chemical trail (pheromone) is left on the ground. The pheromone guides other ants toward the target point. For one ant, the path is chosen according to the quantity of pheromone. The pheromone evaporates over time. If many ants choose a certain path and lay down pheromones, the quantity of the trail increases and thus, this trail attracts more and more ants. The artificial ants simulate the transitions from one point to another point, according to the improved version of ACO, namely the Max-Min AS (MMAS) algorithm presented by Stutzle and Hoos (1998) as follows:

In the ant colony optimization algorithms, ants move in search space to arrive to optimum point. The search space of the ant colony has been shown in Fig. 1. The ant k maintains a black list (N_r^k) in memory that defines the set of points still to be visited when it is at point r. The ant chooses to go from point r to point s during a tour with relation Eq. 1 given by Di Caro and Dorigo (1998).

$$p(r,s) = \frac{\gamma(r,s)}{\sum_{l} \gamma(r,l)} \quad s,l \in N_l^k \tag{1}$$

where, matrix represents the amount of the pheromone trail (pheromone intensity) between points r and s.

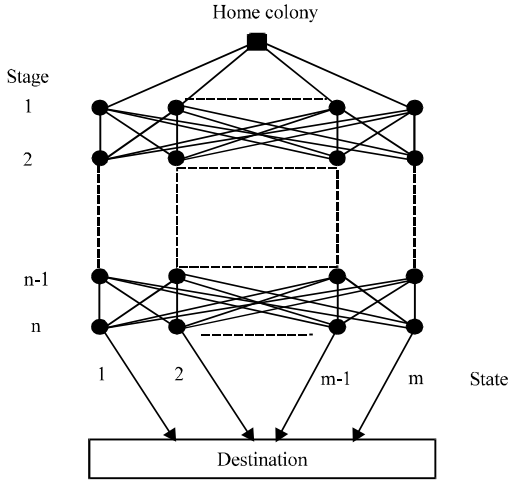

Fig. 1: Search space for an optimization problem

Then, the pheromone trail on coupling is updated according to Eq. 2:

$$\gamma(r,s) = \alpha.\gamma(r,s) + \Delta\gamma^k(r,s) \tag{2}$$

where, α with $0<\alpha<1$ is the persistence of the pheromone trail, so that $(1-\alpha)$ to represent the evaporation and is the amount of pheromone that ant k puts on the trail. The pheromone update $\Delta\gamma^k(r,s)$ reflects the desirability of the trail (r,s), such as shorter distance, better performance, etc., depending on the application problem. Since, the best tour is unknown initially, an ant needs to select a trail randomly and deposits pheromone in the trail, where the amount of pheromone will depend upon the pheromone update rule. The randomness implies that pheromone is deposited in all possible trails, not just in the best trail. The trail with favorable update, however, increases the pheromone intensity more than other trails. After all ants have completed their tours, global pheromone is updated in the trails of the ant with the best tour executed. In the next section, the MMAS algorithm is extended and modified to find optimal or near optimal generator parameters.

Machine structure: In this study, a low speed, Y-connected RFPM generator has been designed and investigated. The generator structure is formed from stator, rotor, winding and PMs. The machine consists of an intermediate rotor with 40 rare-earth PMs and nonmagnetic supporting structure. As a result, the used PM volume is efficiently applied in this structure. The structure of direct-drive generator is shown in Fig. 2.

Because of using low speed generator, the topology shown in Fig. 2 does not need any gearbox to couple to

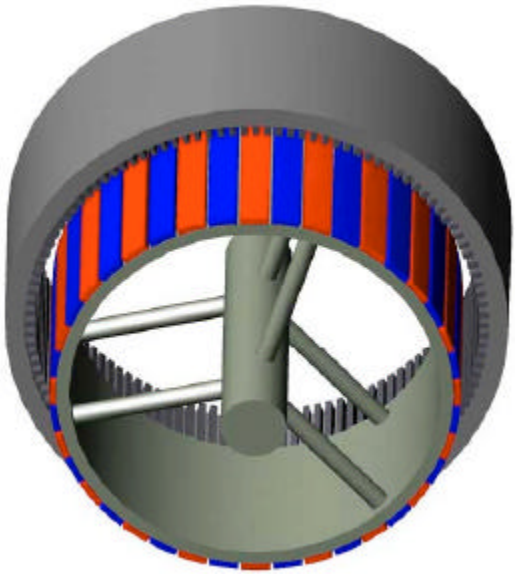

Fig. 2: The structure of the direct-drive RFPM generator

wind turbine. The machine is free of mechanical noise and losses. The cogging torque is decreased with accurate design. In this generator, current density is chosen so that the natural cooling system is sufficient to work in the thermal limit.

Because of the absence of gearbox, it was estimated that considerable input wind energy could be saved for electrical generation. Malekian and Monfared (2007) presented computer-programmed inverter which controlled the hybrid system, the use of normal damp structure is not necessary in the machine. Reliable and simple mechanical construction makes this sort of machine compact and easy to be installed on the top of a tower.

The parameters of the RFPM generator structure, such as PM dimensions and rotor diameter, are optimized.

OPTIMIZATION

Ant colony Optimization (ACO) algorithms are exploratory search and optimization procedures that work base on the behavior of real ants. In this study, ACO and FEM structural programs are used to achieve high power density and efficiency. In the other words, the permanent magnet dimensions and diameter of stator and rotor are optimized using ACO to achieve the above-mentioned objectives. The generator parameters which should be optimized are the thickness, the width and the length of PM as well as the diameter of stator and rotor. The relation Eq. 3 shows fitness function which is utilized to cover such objectives.

$$\Delta\gamma^{k}(r,s) = \frac{1}{Hf} \tag{3}$$

where, H is a large positive constant and f is the objective function which is defined in relation Eq. 4:

$$f = \eta + \xi \tag{4}$$

where, η is the generator efficiency; ξ is the normalized power density which is defined in relation Eq. 5:

$$\xi = \left(\frac{P/m}{\xi_{max}}\right) \tag{5}$$

where, P is the rated power of generator; m is the total mass of generator and ξ_{max} is the maximum possible ξ according to the constraints of the optimization problem which is considered as follows:

$$\begin{aligned} &2\text{ mm} < T_{PM} < 20\text{ mm}\\ &40\text{ mm} < W_{PM} < 80\text{ mm}\\ &100\text{ mm} < L_{PM} < 500\text{ mm}\\ &500\text{ mm} < D < 1000\text{ mm} \end{aligned}$$

where, T_{PM} is the thickness of PM; W_{PM} is the width of PM; L_{PM} is the length of PM and D is the diameter of stator and rotor. These constraints are chosen by considering some practical purposes like the mechanical strength requirements, etc.

A decision variable x_i is represented by a real number within its lower limit a_i and upper limit b_i, i.e., $x_i \in [a_i, b_i]$.

A two-point crossover operator has been employed in this study. The non-uniform mutation operator has been applied in this work. The new value x'_i of the parameter x_i after mutation at generation t is given in relation Eq. 6 and 7:

$$x_i' = \begin{cases} x_i + \Delta(t, b_i - x_i) & \text{if } \tau = 0 \\ x_i - \Delta(t, x_i - a_i) & \text{if } \tau = 1 \end{cases} \tag{6}$$

and

$$\Delta(t,y) = y\left(1 - r^{\left(1-\frac{t}{g_{max}}\right)^{\beta}}\right) \tag{7}$$

where, τ is a binary random number, r is a random number $r \in [0,1]$, g_{max} is the maximum number of point and β is a positive constant chosen arbitrarily. In this study, $\beta = 5$ was selected. This operator gives a value $x'_i \in [a_i, b_i]$ such that the probability of returning a value close to x_i increases as the algorithm advances. This makes uniform search in the initial stages and very locally at the later stages.

After running ACO algorithm, the following optimal parameters have been obtained for constructing the generator:

$$T_{PM} = 10 \text{ mm},\ W_{PM} = 64 \text{ mm},\ L_{PM} = 300 \text{ mm}, D = 516 \text{ mm}$$

FEM simulation: For the modeling purpose, the equivalent 2-dimensional (2-D) model for FEM analysis is used. Figure 3 shows the triangular sections for finite element analysis. The sections density in air gap is more than others. The 2-D FEM analysis is applied to this model. Simulation software generates flux line distribution, flux density distribution which is obtained by PMs. The distribution of flux line is shown in Fig. 4 in no-load conditions. We can see the maximum flux density in air gap section. The maximum flux value in air gap section is between 7.2 and 7.8 mWb. Also, Fig. 5 shows the flux density in no load condition. The maximum flux density in air gap is about 0.7 T. This value is completely ideal in coreless schemes. Because of the optimized design, we can have the maximum flux density in air gap section. In this condition, Rare-earth magnets are able to create an average working flux density of about 1.2 T at the winding.

In order to calculate the induced EMF, an external circuit is connected so that deriving characteristics at a resistive load is analyzed. In the no load state, software calculated the flux linkage and electromagnetic force in winding position. The phase voltage and flux linkage for the resistive load are shown in Fig. 6a and b. The differential angel between voltage and flux is about 89.4 degree. Figure 6 proves that EMf is the integral of the flux linkage. Figure 6 shows that the shape of phase voltage is almost sinusoidal and has more less harmonics in compare to conventional generators.

Using 2-D FEM analysis, both mutual and leakage fluxes can be taken into account. The only remaining part is the end winding leakage flux which is thoroughly discussed by Atallah *et al.* (1998) and Kamper *et al.* (1996).

With the 2-D finite element solution, the magnetic vector potential $\vec{A}$ has only a z component, i.e., $\vec{A} = A(x,y).\hat{a}_z$ where, $\hat{a}_z$ is the unit vector in z direction. The total stator flux of a phase winding ψ_{abc} that excludes the end-winding flux leakage can be readily calculated by using Stokes' theorem, i.e.,

$$\psi_{abc} = \int_s \vec{B}.d\vec{S} = \int_s \vec{\nabla} \times \vec{A}.d\vec{S} = \oint_c \vec{A}.d\vec{l} \quad (8)$$

where, $\vec{B}$ is magnetic flux density.

In the case that the coil is not very thin, magnetic vector potential varies in the coil cross-section area. Therefore, the average magnetic vector potential values should be used. For first order triangular elements, the flux linkage of a coil with N_l turns, area S and length *l* is calculated with relation Eq. 9 which is given by Atallah *et al.* (1998):

$$\psi = N_l \sum_{j=1}^{n} \frac{\Delta_j}{S} \left[\frac{\zeta}{3} \sum_{i=1}^{3} A_{ij} \right] l \quad (9)$$

Fig. 4: Flux line distribution in optimized RFPM generator

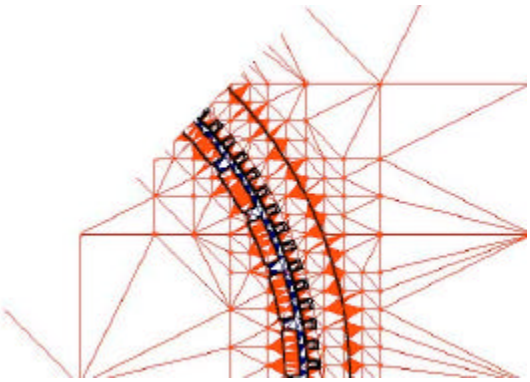

Fig. 3: Mesh distribution in 2-D FEM analysis

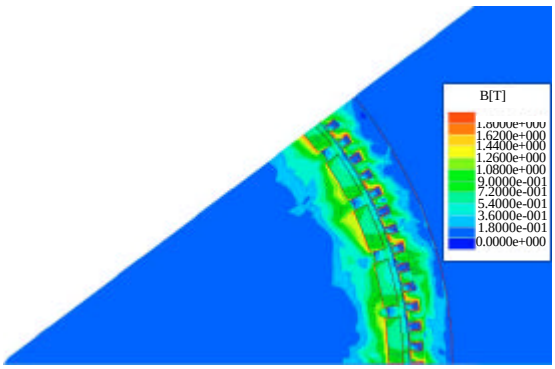

Fig. 5: Flux density in optimized RFPM generator

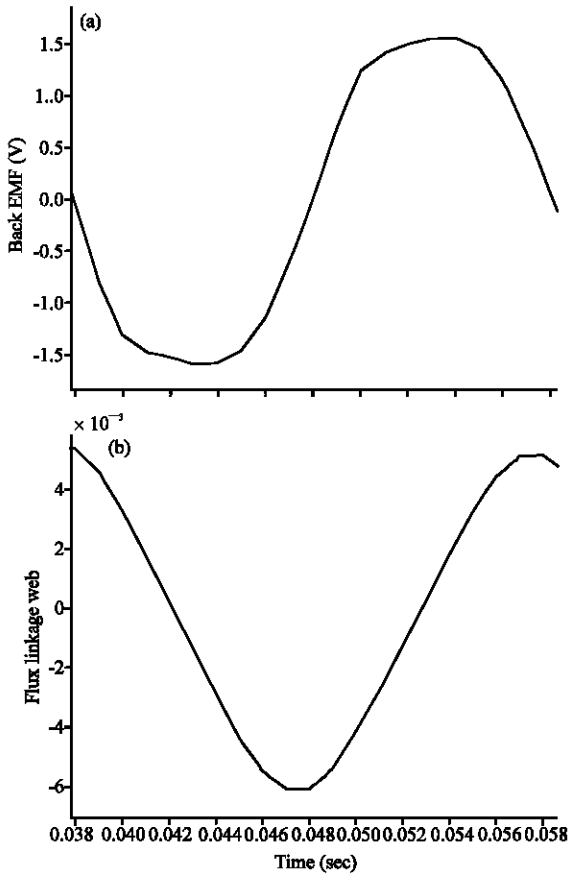

Fig. 6: (a) Back EMF and (b) Flux leakage in optimized RFPM generator

where, A_{ij} is the nodal value of the magnetic vector potential of the triangular element j, ζ = +1 or ζ = -1 indicates the direction of integration either into the plane or out of the plane, Δ_j is the area of the triangular element j and n is the total number of elements of the in-going and out-going areas of the coil. It follows that for an AFPM machine with only one pole modeled, the total flux linkage of a phase winding is calculated by relation Eq. 10:

$$\psi_{abc} = \frac{2PN_l l}{a_p S}\sum_{j=1}^{u}\left[\frac{\Delta_j \zeta}{3}\sum_{i=1}^{3} A_{ij}\right] \quad (10)$$

where, u is the total number of elements of the meshed coil areas of the phase in the pole region and a_p is the number of parallel circuits (parallel current paths) of the stator windings.

If the 5th and 7th and higher harmonics are ignored, the fundamental total phase flux linkages can bee calculated by using the ralation Eq. 11 which is given by Atallah *et al.* (1998), i.e.,

$$[\psi_{abc1}] \approx [\psi_{abc}] - [\psi_{abc3}] \quad (11)$$

where, the co-phasal 3rd harmonic flux linkage, including the higher order triple harmonics, can be obtained from relation Eq. 12:

$$\psi_{a3} = \psi_{b3} = \psi_{c3} \approx \frac{\psi_{a3} + \psi_{b3} + \psi_{c3}}{3} \quad (12)$$

With the fundamental total phase flux linkages and rotor position known, the d- and q-axis flux linkages are calculated using Park's transformation as relation Eq. 13 and 14 which is given by Hughes and Miller (1997):

$$[\psi_{dq0}] = [K_p][\psi_{abc1}] \quad (13)$$

where,

$$K_p = \frac{2}{3}\begin{bmatrix} \cos\theta & \cos(\theta - \frac{2\pi}{3}) & \cos(\theta + \frac{2\pi}{3}) \\ -\sin\theta & -\sin(\theta - \frac{2\pi}{3}) & -\sin(\theta + \frac{2\pi}{3}) \\ \frac{1}{2} & \frac{1}{2} & \frac{1}{2} \end{bmatrix} \quad (14)$$

In this type of generator, the d-axis and q-axis synchronous inductances are equal and are defined as relation Eq. 15,

$$L_{sd} = L_{sq} = L_l + L_m + L_{ew} \quad (15)$$

where, L_l is the leakage inductance; L_m is mutual inductance and L_{ew} is the end winding inductance. Sum of the leakage and mutual inductances is calculated using relation Eq. 16:

$$L_l + L_m = \frac{\psi_d - \psi_f}{i_{ad}} = \frac{\psi_q}{i_{aq}} \quad (16)$$

where, ψ_d and ψ_q are the d- and q-axis flux, respectively; i_{ad} and i_{ad} are the d- and q-axis current, respectively; ψ_f is the flux of PM on the d-axis.

The end winding inductance, L_{ew}, can be calculated using relation Eq. 17 from numerical evaluation of the energy stored in the end connection.

$$L_{ew} = 2\mu_0 \frac{N_1^2 l_{1ew}}{Pq_1}\lambda_{1ew} \quad (17)$$

where, q_1 is the number of coil sides per pole per phase; l_{1ew} is the length of the one-sided end connection and λ_{1ew} is the specific permeance for the leakage flux about the end connection.

IMPLEMENTATION

In this study, a low speed, Y-connected RFPM generator rated at 20 kW, 150 rpm has been constructed after designing and optimizing. The stator three-phase winding fixed to the stator frame is assembled as flower petals. Multi-turn coils for each pole are arranged in overlapping layers around the shaft-axis of the machine. The whole winding is then embedded integrity resin. Forty average-quality nickel-coated sintered NdFeB PMs with B_r = 1.2 T and H_c = 950 kA/m have been used in rotor surface. Table 1 shows specifications of the constructed optimized RFPM direct-drive generator.

The constructed AFPM generator has been tested as a stand alone a.c. generator. The experimental setup for testing this generator is shown in Fig. 7. The shaft of the generator and the shaft of the prime mover, which is a d.c. machine, are coupled together via a torque meter. The open circuit characteristic, i.e., EMF (line-to-line), as a function of speed is shown in Fig. 8. The main output of the generator is the voltage waveform which must be sinusoidal. The line-to-line EMF at rated speed (i.e., 150 rpm) is shown in Fig. 9. The actual value in Fig. 9 shows that we will have less harmonic and iron losses in comparison with conventional generators.

Table 1: Specifications of the constructed rfpm direct-drive generator

Parameter	The ironless AFPM generator
Output power (kW)	20
Efficiency (%)	91.4
Power factor	0.86
Number of poles	20
Nominal speed (rpm)	150
Nominal torque (N.m)	1283.8
Nominal phase EMF (V)	220
Winding resistance at 100°C (Ω)	0.085
Winding losses (kW)	0.615
Total losses (kW)	1.72
Winding temperature rise (°C)	32
Maximum winding temperature (°C)	110
Air gap at each side (mm)	1
Mass of complete generator (kg)	280
Stator diameter (mm)	580
Rotor diameter (mm)	516
Power density (W kg^{-1})	71.4
Current density (A mm^{-2})	4.7
Cooling system	Natural

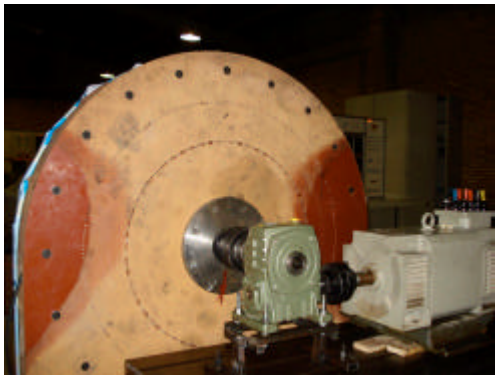

Fig. 7: Constructed RFPM generator setup

MACHINE LOSSES AND EFFICIENCY

Since, the gearbox is not used, in the direct-drive generators, the losses pertaining to the gearbox will be omitted. The aerodynamic loss is proportional to the cube of speed. As a result, compared to the conventional RFPM generators, the aerodynamic loss is considerably less because the rated speed for direct-drive generators is approximately one-tenth of the rated speed of the conventional ones. The main loss in an RFPM generator is the copper loss, RI2. Eddy-current loss in the winding conductors is important because the conductors are exposed in the main field.

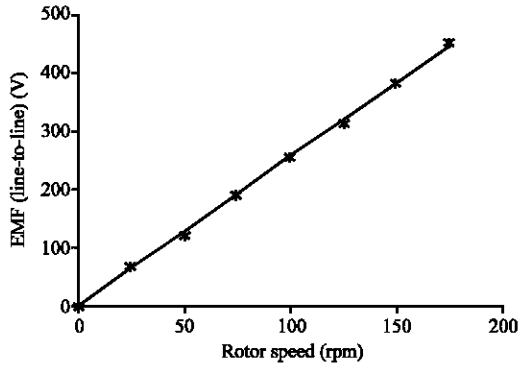

Fig. 8: Open circuit characteristic of the ironless AFPM generator

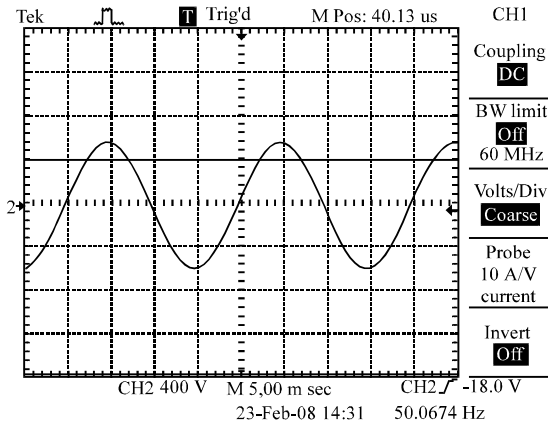

Fig. 9: The line-to-line EMF at 150 rpm for no load condition

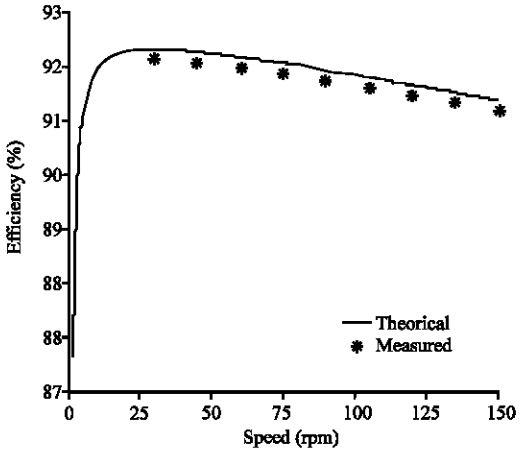

Fig. 10: The theorical and practical efficiencies versus mechanical speed

If the wind speed reduces to k×the rated value (k<1), then each of the above-mentioned loss component varies as follow:

- The input power varies as k3
- The copper loss varies approximately as k4
- The eddy-current loss varies as frequency, hence k4
- the aerodynamic loss varies with the cube of speed, k3

According to the relations between losses and speed variation, the efficiency of an ironless AFPM generator can be written in relation Eq. 18:

$$\eta = \frac{k^3 P_{in} - (P_{cu} k^4 + P_{ed} k^4 + P_{ae} k^3)}{k^3 P_{in}} \quad (18)$$

where, P_{in} is the rated input power; P_{cu} is the rated copper loss; P_{ed} is the rated eddy-current loss and P_{ae} is the rated aerodynamic loss. Efficiency of the generator changes with the change in rotor speed. Figure 10 shows the theorical curve for efficiency versus speed. Also, in some speeds, the efficiency is practically calculated by measuring the output and input power of the generator. The practical data are also shown in Fig. 9. As shown in Fig. 9 there is an appropriate concordance between theorical and practical efficiency.

CONCLUSION

Design and optimization of a high power direct-drive RFPM generator for wind applications are presented in this study. Operation of this generator has been investigated in both finite element simulation and implementation. Also, proper efficiency and power density have been achieved using Ant colony optimization algorithm. Such a high efficiency is a result of decreasing core losses and cogging torque in this ironless structure. These initially promising results were followed by further work involving the development of a prototype generator to validate the design methodology with experimental results and the development of a finite element.

ACKNOWLEDGMENTS

Authors would like to acknowledge the active participation and financial support of the Mapna Electrical and Control Engineering and Manufacturing Company.

REFERENCES

Atallah, K., Z.Q. Zhu, D. Howe and T.S. Brich, 1998. Armature reaction field and winding inductances of slotless permanent-magnet brushless machines. IEEE Trans. Magnetics, 34: 3737-3744.

Boldea, I. and S.A. Nasar, 1987. Permanent-magnet linear altsmaton, Part I: futidimental equations. IEEE Trans. Aerospace Electronic Syst., 23: 73-78.

Chen, J., C.V. Nayar and L. Xu, 2000. Design and finite-element analysis of an outer-rotor permanent magnet generator for directly coupled wind turbines. IEEE Trans. Magn., 36: 3802-3809.

Di Caro, G. and M. Dorigo, 1998. AntNet: Distributed stigmergetic control for communications networks. J. Artif. Intell. Res., 9: 317-365.

Dorigo, M., V. Maniezzo and A. Colorni, 1991. The ant system: an autocatalytic optimizing process. Technical Report TR91-016, Politecnico di Milano.

Dorigo, M., 1992. Optimization, learning and natural algorithms. Ph.D Thesis, Politecnico de Milano, Italy.

Dorigo, M., V. Maniezzo and A. Colorni, 1996. The ant system: Optimization by a colony of cooperating agents. IEEE Trans. Syst. Man Cybernet., 26: 29-41.

Gieras, J.F. and I.A. Gieras, 2002. Performance analysis of a coreless permanent magnet brushless motor. Proc. IEEE 37th IAS Meeting37th IAS Annual Meeting Ind. Appl. Conf., 4: 2477-2482.

Gieras, J.F., R. Wang and M.J. Kamper, 2004. Axial Flux Permanent Magnet Brushless Machine. Kluwer Academic Publishers, New York.

Hughes, A. and T.J. Miller, 1997. Analysis of fields and inductances in Air-cored and Iron-cored synchronous machines. Proc. IEEE, 124: 121-126.

Joorabian, M. and A.N. Zabihinejad, 2009. Design and construction of an optimum high power radial flux direct-drive PM generator for wind applications. Proceedings of the 4th IEEE Conference on Industrial Electronics and Applications, May 25-27, Shahid Chamran University of Ahvaz, pp: 524-529.

Kamper, M.J. and F.S. van der Merwe and S. Williamson, 1996. Direct finite element design optimization of cageless reluctance synchronous machine. IEEE Trans., 11: 547-555.

Kang, D.H., P. Curiac and J. Lee, 2000. An axial flux interior PM synchronous machine. Proc. ICEM, 3: 1475-1479.

Kessinger, R.L. and S. Robinson, 1997. SEMA-based permanent magnet motors for high torque high performance. Proceedings of the Naval Symposium Electric Machines, (NSEM'97), Newport, RI., USA., pp: 151-155.

Kessinger, R.L., P.A. Stahura, P.E. Receveur and K.D. Dockstader, 1998. Interlocking segmented coil array. US. Patent No. 5,744,896. http://www.freepatentsonline.com/5744896.html.

Malekian, K. and J.M. Monfared, 2007. A genetic based fuzzy logic controller for IPMSM drive over wide speed range. Proc. Electric Ma-Chines Drives Conf., 1: 847-853.

Mirzayee, M., H. Bahrami, A. Zabihi and M. Joorabian, 2005. A novel flux-reversal axial flux generator for high speed applications. Proc. Int. Conf. Power Electronics Drives Syst., 2: 1152-1155.

Muljadi, E., C.P. Butterfield and Y.H. Wan, 1999. Axial-flux modular permanent-magnet generator with a toroidal winding for wind-turbine applications. IEEE Trans. Industry Appl., 35: 831-836.

Stutzle, T. and H.H. Hoos, 1998. Improvements on the Ant System: Introducing the MAX-MIN Ant System. Springer Verlag, New York, pp: 245-249.

Tsekouras, G., S. Kiartzis, A.G. Kladas and J.A. Tegopoulos, 2001. Neural network approach compared to sensitivity analysis based on finite element technique for optimization of permanent magnet generators. IEEE Trans. Magn., 37: 3618-3621.